

Article

Photocatalytic Degradation of Tetracycline in Aqueous Solution Using Copper Sulfide Nanoparticles

Murendeni P. Ravele^{1,2}, Opeyemi A. Oyewo³ , Sam Ramaila³ , Lydia Mavuru³ 
and Damian C. Onwudiwe^{1,2,*} 

¹ Material Science Innovation and Modelling (MaSIM) Research Focus Area, Faculty of Natural and Agricultural Sciences, Mafikeng Campus, North-West University, Private Bag X2046, Mmabatho 2735, South Africa; 32470789@nwu.ac.za

² Department of Chemistry, School of Physical and Chemical Sciences, Faculty of Natural and Agricultural Sciences, Mafikeng Campus, North-West University, Private Bag X2046, Mmabatho 2735, South Africa

³ Department of Science and Technology Education, University of Johannesburg, Johannesburg 2092, South Africa; atiba.opeyemi@gmail.com (O.A.O.); samr@uj.ac.za (S.R.); lydiam@uj.ac.za (L.M.)

* Correspondence: Damian.Onwudiwe@nwu.ac.za; Tel.: +27-18-389-2545; Fax: +27-18-389-2420

Abstract: In this paper, spherical-shaped pure phase djurleite ($\text{Cu}_{31}\text{S}_{16}$) and roxbyite (Cu_7S_4) nanoparticles were prepared by a solvothermal decomposition of copper(II) dithiocarbamate complex in dodecanthiol (DDT). The reaction temperature was used to control the phases of the samples, which were represented as $\text{Cu}_{31}\text{S}_{16}$ (120 °C), $\text{Cu}_{31}\text{S}_{16}$ (150 °C), Cu_7S_4 (220 °C), and Cu_7S_4 (250 °C) and were characterized by using X-ray diffraction (XRD), scanning and transmission electron microscopy (SEM and TEM), and absorption spectroscopy. The samples were used as photocatalysts for the degradation of tetracycline (TC) under visible light irradiation. The results of the study showed that Cu_7S_4 (250 °C) exhibited the best activity in the reaction system with the TC degradation rate of up to 99% within 120 min of light exposure, while the $\text{Cu}_{31}\text{S}_{16}$ (120 °C) system was only 46.5% at the same reaction condition. In general, roxbyite Cu_7S_4 (250 °C) could be considered as a potential catalyst for the degradation of TC in solution.

Keywords: copper sulfide; tetracycline; djurleite; roxbyite; photodegradation



Citation: Ravele, M.P.; Oyewo, O.A.; Ramaila, S.; Mavuru, L.; Onwudiwe, D.C. Photocatalytic Degradation of Tetracycline in Aqueous Solution Using Copper Sulfide Nanoparticles. *Catalysts* **2021**, *11*, 1238. <https://doi.org/10.3390/catal11101238>

Academic Editors: Paola Semeraro and Roberto Comparelli

Received: 30 August 2021

Accepted: 7 October 2021

Published: 14 October 2021

Publisher's Note: MDPI stays neutral with regard to jurisdictional claims in published maps and institutional affiliations.



Copyright: © 2021 by the authors. Licensee MDPI, Basel, Switzerland. This article is an open access article distributed under the terms and conditions of the Creative Commons Attribution (CC BY) license (<https://creativecommons.org/licenses/by/4.0/>).

1. Introduction

Antibiotics are generally used to prevent and also treat microbial infections by either killing or inhibiting their growth. They are important for the control, prevention, and treatment of diseases in both humans and animals. In most developed nations, it is estimated that livestock alone consumes between 50 and 80% of antibiotics produced [1]. These antibiotics could be divided into aminoglycosides, quinolone, sulfonamides, macrolides, and tetracycline based on their structures [2]. The misuse of antibiotics has a huge negative impact on environmental contamination, especially on soil and water resources. Some traces of antibiotics have been detected in sewage, ground, surface, and drinking water [3,4]. The persistence of antibiotics in the environment could result in the development of their resistance in microorganisms [5,6], and tetracycline (TC) has been reported as one of the most widely used antibiotics [7].

TC is an amphoteric compound that contains four connected rings consisting of different active functional groups including alcohol, aldehyde, and phenol, with three ionizable groups: tricarbonylamide, dimethyl amino, and phenolic-diketone groups. These allow TC to ionize with three dissociation constants with pKa values of 3.3, 7.7, and 9.7. Thus, anionic, cationic and zwitterionic species exist under alkaline, acidic, and moderately acidic to neutral conditions, respectively [8,9]. It is widely used in humans to treat bacterial infections and also in animal feed as a growth promoter [10]. Most of the administrated

TC is relatively poorly adsorbed by animals or humans; therefore, their metabolites are excreted through feces and urine into the environment. Once in the environment, they can lead to the development of multi-resistant bacterial strains, which cannot be treated with the common known drugs [11,12]. These possible risks make it of great importance to explore feasible and cost-effective techniques for the removal of TC.

The removal of TC from water by different methods such as adsorption [13,14], biological [15] degradation, and chemical degradation have been studied. However, their high cost and low removal efficiency usually limit their applications. Photocatalysis is a promising technique due to its low cost and efficiency. Different semiconductor nanomaterials have been used as photocatalysts either in their pure forms or as composite to affect the degradation of TC. For example, TiO_2 [16], $\text{g-C}_3\text{N}_4$ [17], ZnS [18], and BiVO_4 [19] have been used to achieve the removal of TC from aqueous solution. The use of binary composites such as $\text{ZnO/g-C}_3\text{N}_4$ [20], $\text{FeNi}_3\text{/SiO}_2$ [21], $\text{Sr-Bi}_2\text{O}_3$ [22], SnO/CeO_2 [23], and $\text{ZnO}/\gamma\text{-Fe}_2\text{O}_3$ [24] or ternary composites including MGO-Ce-TiO_2 [25], $\text{CeO}_2/\text{Bi}_2\text{O}_2\text{CO}_3$ [26], $\text{Ag/Ag}_2\text{CO}_3\text{/BiVO}_4$ [27], and $\text{IO-TiO}_2\text{-CdS}$ [28] have also been reported. However, due to some demerits associated with some of these materials such as high cost, economical non-viability, and poor efficiency, there is a need to explore other semiconductors. For example, despite the great advantages of TiO_2 , its shortcomings include activation within the UV range only (due to a large band gap of 3–3.2 eV), fast recombination between electron–hole pairs, and high tendency for agglomeration. The modification of TiO_2 before its use as a photocatalyst is one of the methods used to address these shortcomings. Consequently, a non-toxic semiconductor nanomaterial such as copper sulfide is a good alternative, as it is relatively cheap, has good light absorption properties over a wide range of wavelengths, and exhibits different crystalline phases [29] that could open up wide areas of application. Compared with other semiconductor materials, copper oxide has not been explored in the photocatalytic degradation of TC.

Copper sulfide is a p-type indirect band-gap semiconductor material and occupies a very significant position within the family of compound semiconductors. The p-type conduction property is ascribed to the free holes, which is generated from the acceptor levels of copper vacancies [30]. It is reported to exhibit size-dependent properties that are similar to the widely explored lead and cadmium systems, and it has the advantage of being a non-toxic material. In addition, the earth-abundance nature of its constituent elements makes it a very promising candidate for the fabrication of devices [31]. Another interesting properties of copper sulfide is its existence in variable stoichiometries. This makes it a very interesting compound for fundamental studies, possessing different band-gap energies and electronic properties. The different stoichiometric phases of copper sulfide range from the copper-rich phases: chalcocite (Cu_2S), djurleite ($\text{Cu}_{31}\text{S}_{16}$ or $\text{Cu}_{1.94}\text{S}$), digenite (Cu_9S_5 or $\text{Cu}_{1.8}\text{S}$), and anilite/roxbyite (Cu_7S_4 or $\text{Cu}_{1.75}\text{S}$) to the copper-poor phases: covellite (CuS) and villamaninite (CuS_2) [30,32]. The variation in stoichiometry also influences their band-gap energies. For instance, while the chalcocite has an indirect bulk band-gap energy of ≈ 1.2 eV, the digenite phase possesses a band-gap energy of 1.5 eV [33], and this is favorable for the absorption of light under sunlight illumination.

The synthesis of well-defined pure phase colloidal copper sulfide is a challenge, and the very close relationship that exist between properties and shapes implies that tailoring of the morphology of nanostructures is critical in the synthesis of desired materials with specific properties. Herein, a facile solvothermal method is reported for the synthesis of pure djurleite and roxbyite phases using copper(II) dithiocarbamate (CuDTC) as a single-source precursor and dodecanthiol (DDT) as surfactants. CuDTC was utilized as the single-source precursor due to its ease of synthesis, good stability, and ability to undergo sharp decomposition with less impurity. By changing the reaction temperature during the decomposition process of the complex, it was possible to alter the nucleation and growth process of the copper sulfide nanoparticles, thereby manipulating their optical and structural properties. The as-prepared copper sulfides were air-stable; hence, the obtained

pure phases of djurleite ($\text{Cu}_{31}\text{S}_{16}$) and roxbyite (Cu_7S_4) were used as photocatalysts for the degradation of tetracycline in aqueous solution.

2. Results

2.1. Structural Studies

The phase structures of the as-synthesized nanoparticles at different reaction temperatures were investigated using XRD and presented in Figure 1. The temperature of synthesis of copper sulfide determines the composition and stoichiometry. In the samples obtained at 120 and 150 °C, the peaks at $2\theta = 37.53, 46.31, 48.63,$ and 54.22 °C correspond to the $(-4\ 2\ 5), (10\ 5\ 2), (-2\ 8\ 2),$ and $(2\ 6\ 6)$ planes, respectively, of monoclinic djurleite $\text{Cu}_{31}\text{S}_{16}$ with a space group of $P21/n (14)$ (JCPDS No. 034-0660) [34]. Our previous report involving the same complex but in oleylamine as solvent yielded pure phase covellite at lower temperature and digenite at higher temperature [35]. Similar studies involving the thermal decomposition of Bis(O-alkylxanthato)copper(II) in oleylamine showed the formation of djurleite ($\text{Cu}_{31}\text{S}_{16}$) phase as either an impurity phase or as the secondary phase. The results further showed the dependence of copper sulfide phases on the factors such as precursor type, growth temperature, and synthesis method used [36].

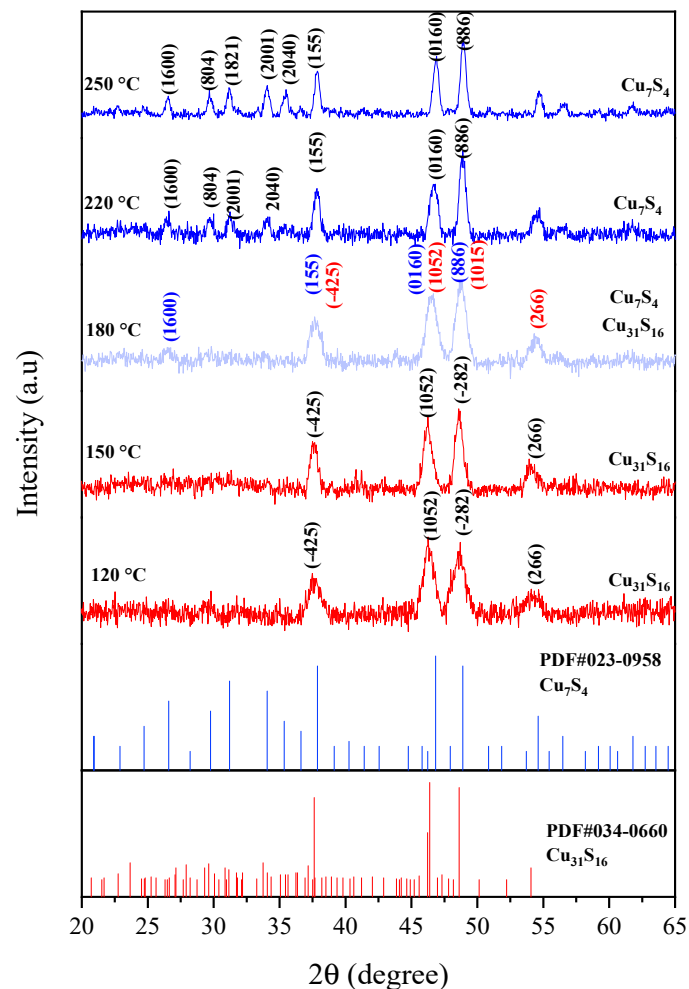


Figure 1. Overlapped XRD patterns for the various phases of copper sulfide obtained at different synthesis temperatures.

As the reaction temperature was increased to 180 °C, the diffraction peaks of base-centered monoclinic Cu_7S_4 could be observed at $2\theta = 26.53, 37.53, 46.50,$ and 48.72° , showing that the roxbyite, syn phase of copper sulfide was beginning to form and may be generated at higher temperature. The formation of pure phase Cu_7S_4 was confirmed at

220 °C, with the diffraction peaks at $2\theta = 26.44, 29.62, 37.82, 46.70,$ and 48.82° attributed to the (16 0 0), (8 0 4), (1 5 5), (0 16 0), and (8 8 6) of roxbyite, syn (JCPDS No. 00-023-0958). XRD results for the two samples at 220 and 250 °C matched very well with the reported data of roxbyite [37,38]. Obviously, the higher reaction temperature favored the phase transformation to the roxbyite phase, which perhaps was governed by the thermodynamic process. Furthermore, the formation of the Cu_7S_4 phase at higher temperature than the $\text{Cu}_{1.95}\text{S}$ phase was a confirmation of the difference in their stability temperature. Apart from the variation of the temperature, a solvent system has also been used to alter the stoichiometry of the product in a solvothermal process involving the use of single-source precursors. For instance, Shen et al. [39] reported the formation of hexagonal phase Cu_2S nanocrystals by the thermal decomposition of copper diethyldithiocarbamate at 220 °C when DDT was used as surfactant. However, a change in the solvent system to oleic acid (OA) yielded pure monoclinic phase Cu_7S_4 (JCPDS: 23-0958).

2.2. Morphological Studies by Electron Microscopy

The effects of reaction temperature on the size, morphological transformation, and also the growth of the nanoparticles was studied by scanning and transmission electron microscopies. Figure 2a,b show the SEM images of the pure djurlerite and roxbyite phases, respectively. Reaction temperature is a key factor in the controlled synthesis of colloidal inorganic nanoparticles [39–41]. The image showed that the samples were spherical even as the temperature was extended to 150 °C. The formation of spherical nanoparticles in all the samples, as shown by the TEM images, could be ascribed to the ability of DDT as a surfactant to non-selectively adsorb on the surface of the crystal facets upon nucleation; thereby, it passivated all the surfaces of the crystal facets indiscriminately. This process successfully prohibited the facets from excessive growth and resulted in the isotropic growth of the nanoparticles.

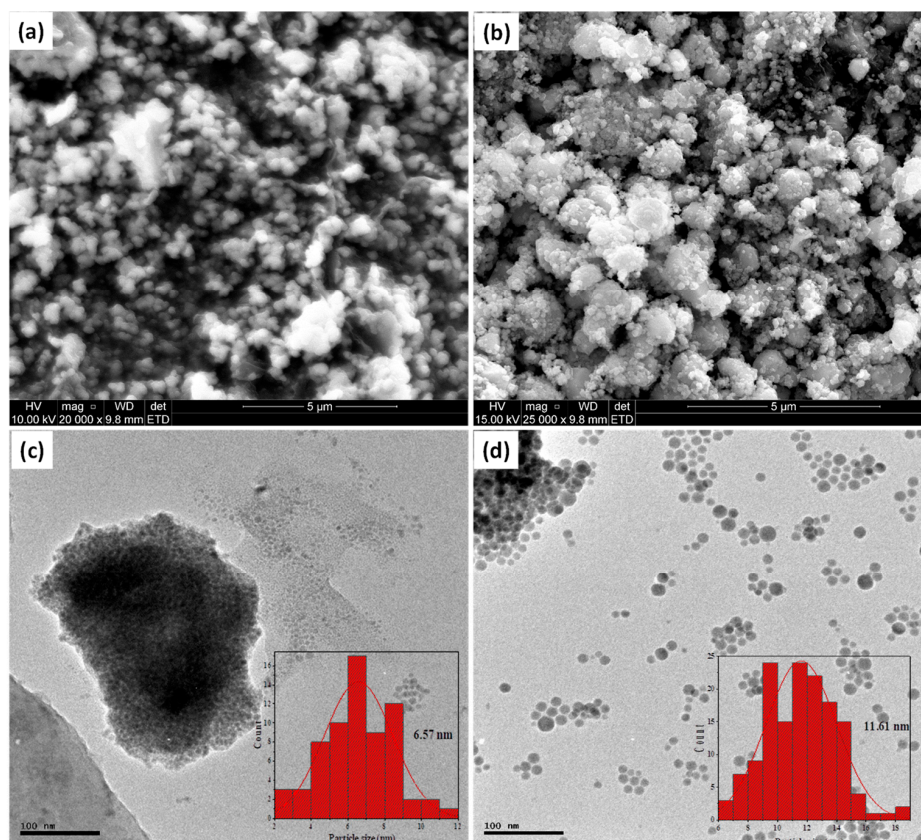


Figure 2. SEM images of (a) $\text{Cu}_{31}\text{S}_{16}$ (120 °C) and (b) $\text{Cu}_{31}\text{S}_{16}$ (150 °C); TEM images of (c) $\text{Cu}_{31}\text{S}_{16}$ (120 °C) and (d) $\text{Cu}_{31}\text{S}_{16}$ (150 °C). Insets are the respective particle size distribution histogram.

In addition, the DDT played other roles during the thermal decomposition process of the copper complex precursor. It also acted as sulfur donor, promoting the formation of sulfur-rich nanoparticles and it is also responsible for triggering the decomposition process of the single-source precursors at relatively low temperature. This was important, as it facilitates the separation of the nucleation process from the growth process, which is a critical factor for the development of high-quality nanoparticles. For example, the thermal decomposition temperature of the CuDTC was lowered from 260 °C in solid state to 120 °C in the presence of DDT in solution, similar to previous report using oleylamine as surfactant [42]. The micrographs showed no change in the morphology of the samples at both temperatures (120 and 150 °C), but as presented in the particle size distribution histogram, an increase in the average nanoparticles size from 6.57 to 11.67 nm occurred as the reaction temperature was increased from 120 to 150 °C.

Apart from the single-source precursor method's advantage of being able to control the size and morphology of the nanoparticles through the choice of surfactants used in the reaction system, it also has the potential to control the chemical composition of the product in cases such as copper sulfide, which has various stoichiometric compositions. As shown in Figure 3a,b, the roxbyite obtained at 220 and 250 °C consisted of quasi-spherical nanoparticles even as the reaction temperature was increased, and the TEM images presented in Figure 3c,d indicated, at a closer observation, that the morphology seemed to be tending toward hexagons. The alteration of morphology from a distinct spherical structure to a quasi-spherical structure, with temperature increase, showed that the phase variation was associated with shape changes. The particles size distribution histogram showed a size increase from 24.2 nm at 220 °C to 26.4 nm at 250 °C, again indicating that the increase in particle growth occurred with the temperature increase.

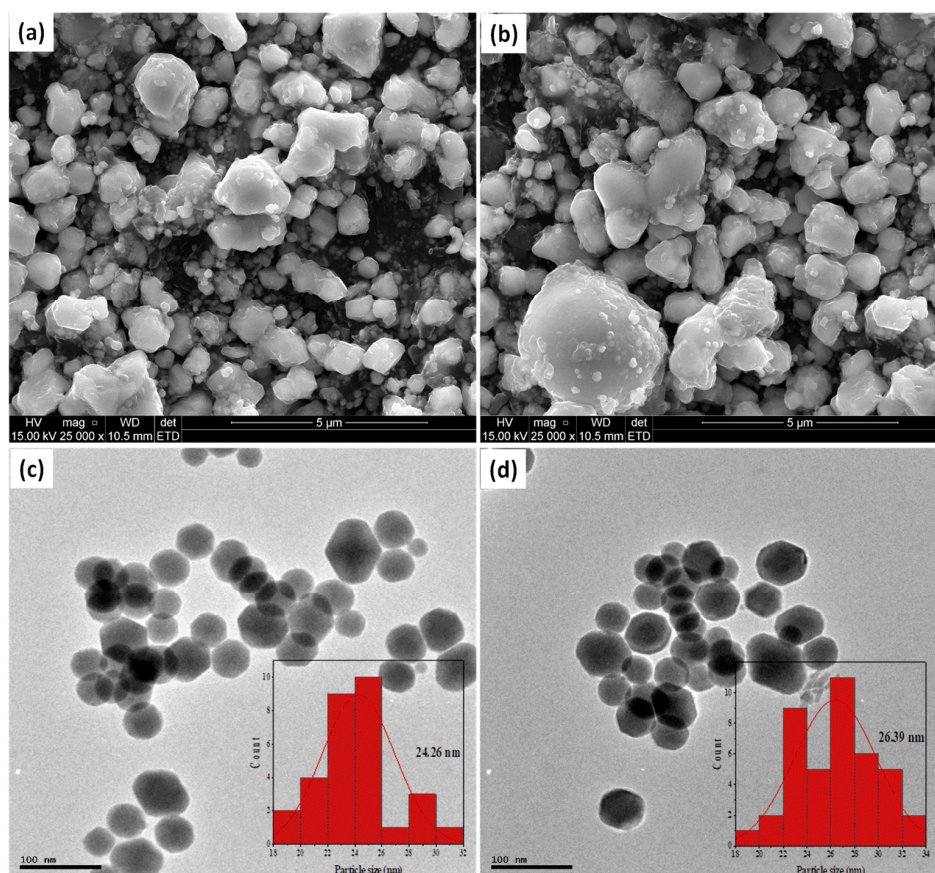


Figure 3. SEM images of (a) Cu_7S_4 (220 °C) and (b) Cu_7S_4 (250 °C); TEM images of (c) Cu_7S_4 (220 °C) and (d) Cu_7S_4 (250 °C). Insets are the respective particle size distribution histogram.

2.3. Brunauer, Emmett, and Teller (BET) Surface Area Analysis

The specific surface areas of Cu₃₁S₁₆ (120 °C), Cu₃₁S₁₆ (150 °C), Cu₇S₄ (220 °C), and Cu₇S₄ (250 °C) were investigated by the Brunauer–Emmett–Teller (BET) method, and the results obtained are summarized in Table 1. According to the adsorption isotherm classification of BET, the material was found to be a mesoporous structure. This is due to the presence of more surface active sites on the copper sulfide nanoparticles. The result revealed that the specific surface area of copper sulfide nanoparticles of Cu₃₁S₁₆ (120 °C), Cu₃₁S₁₆ (150 °C), Cu₇S₄ (220 °C), and Cu₇S₄ (250 °C) was found to be 14.98, 15.45, 16.95, and 17.32 m²/g, while their pore sizes are in the range 17.62 to 18.52 nm. Although, the spherical shapes of these photocatalysts affect their BET values, the structure and specific surface area were favorable for the adsorption of TC [43].

Table 1. BET analysis of copper sulfide photocatalyst samples.

Sample Name	Surface Area (m ² /g)	Pore Diameter (nm)	Pore Volume (m ³ /g)
Cu ₃₁ S ₁₆ (120 °C)	14.98	17.62	0.074
Cu ₃₁ S ₁₆ (150 °C)	15.45	17.45	0.077
Cu ₇ S ₄ (220 °C)	16.95	18.23	0.085
Cu ₇ S ₄ (250 °C)	17.32	18.52	0.087

2.4. Absorbance Studies

The absorption spectra of the synthesized djurleite and roxbyite phases at different temperatures are shown in Figure 4. It shows some similarities in the spectra of the djurleite (120 and 150 °C) (Figure 4a,b). Likewise, similar absorption spectra could be observed in the pattern of the roxbyite phase (220 and 250 °C) in Figure 4c,d. The djurleite phases show a broad peak from 300 to around 600 nm, while the roxbyite phases showed a narrow peak around 260 nm, which reaches a maximum around 450 nm and declines to minimum at ≈650 nm. In all the phases, the absorbance never reaches zero intensity, even in their minimum, but it rises again toward the longer wavelengths region, and this is thought to arise due to the free-carrier intraband absorbance [44]. The absorbance of the roxbyite phases in this longer wavelength region is stronger than the djurleite phases and may be due to free-carrier absorbance [45]. Considering that this NIR absorbance derives from free carriers, it should exhibit a stoichiometric dependence, and the observed behavior could be rationalized on this basis. In the spectrum of the djurleite at 120 °C, an absorption shoulder around 900 nm could be observed. This corresponds to the band-gap energy of 1.36 eV and is attributed to the band-edge absorption of the nanoparticles.

The band-gap energies were determined by using Tauc relation:

$$\alpha hv = \beta(hv - E_g)^n$$

where hv is the photon energy, α is the absorption coefficient i.e., $\alpha = \frac{2.303A}{t}$, and β is the band edge. The n value can be 2 or 0.5 for a direct or indirect transition, respectively [46]. The values for the optical band gaps were found to be 1.34, 1.38, 2.14, and 2.20 eV for Cu₃₁S₁₆ (120 °C), (b) Cu₃₁S₁₆ (150 °C), (c) Cu₇S₄ (220 °C), and (d) Cu₇S₄ (250 °C), respectively (inserts). These values are comparable to other similar studies [47,48] and also indicated a shift to a shorter wavelength compared to the band-gap energy of their bulks [44,49].

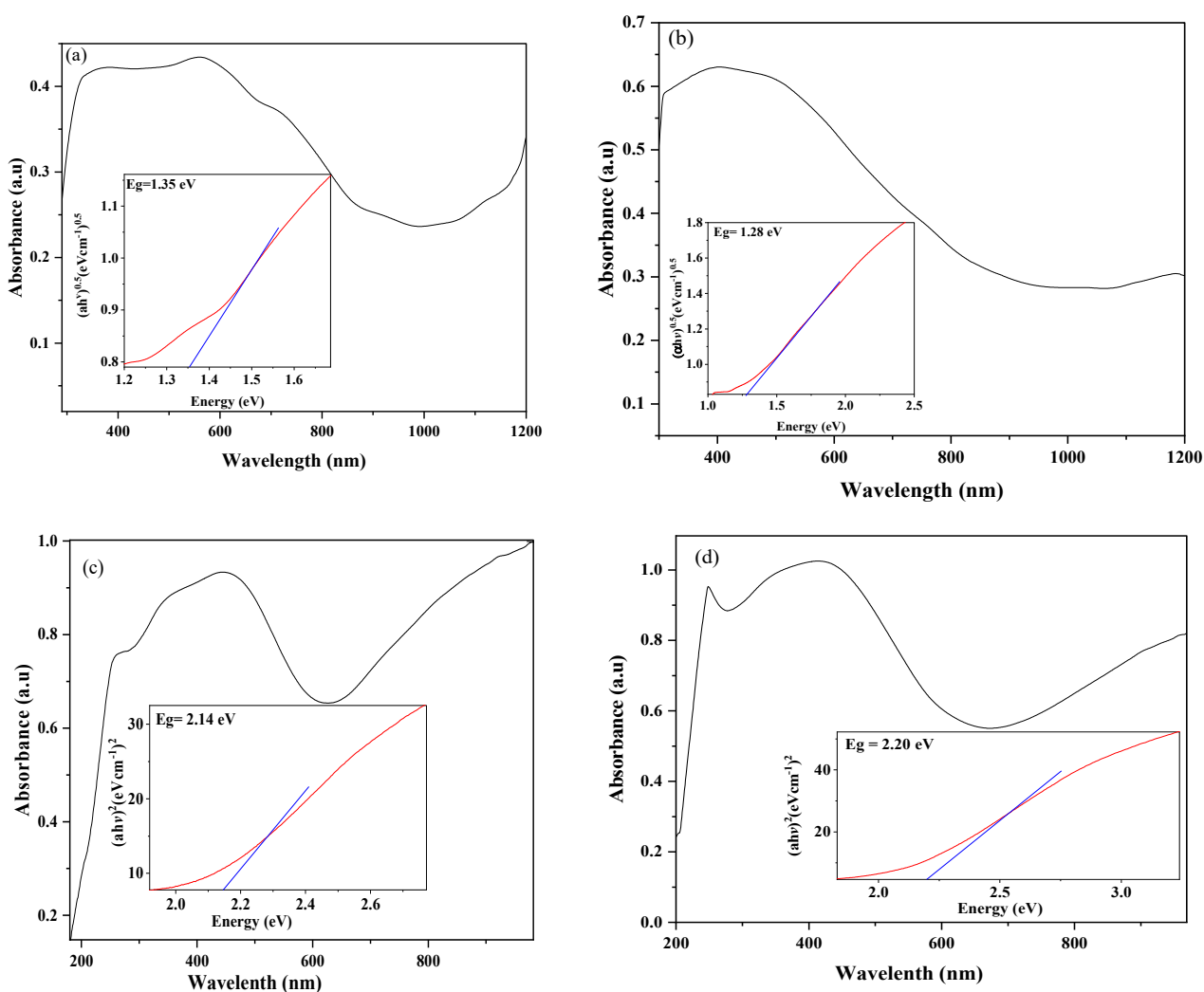


Figure 4. UV-vis-NIR spectra of (a) $\text{Cu}_{31}\text{S}_{16}$ (120 °C), (b) $\text{Cu}_{31}\text{S}_{16}$ (150 °C), (c) Cu_7S_4 (220 °C), and (d) Cu_7S_4 (250 °C). The insets are the respective Tauc plots.

2.4.1. Photocatalytic Degradation of TC Using Roxbyite and Djulerite

The photocatalytic degradation of TC solution using the pure phase samples ($\text{Cu}_{31}\text{S}_{16}$ (120 °C), $\text{Cu}_{31}\text{S}_{16}$ (150 °C), Cu_7S_4 (220 °C), and Cu_7S_4 (250 °C)) was conducted under the visible light irradiation. In the absorption spectrum of aqueous solution of TC, two absorption bands at approximately 275 and 360 nm are ascribed to the conjugated double-bond structures with two carbonyl groups and enolic groups, respectively [50]. The absorption spectra of tetracycline using $\text{Cu}_{31}\text{S}_{16}$ (120 °C), $\text{Cu}_{31}\text{S}_{16}$ (150 °C), Cu_7S_4 (220 °C), and Cu_7S_4 (250 °C) as catalysts are shown in Figure 5a–d respectively. The figure showed that the two phases of the copper sulfide nanoparticles, roxbyite- Cu_7S_4 and djulerite- $\text{Cu}_{31}\text{S}_{16}$, irrespective of their difference in synthesis temperature, have similar degradation patterns. During the photocatalysis processes, a non-sequential decrease and a slight shift of the absorption peak at greater wavelengths were observed with the increase in irradiation time up to 120 min. The two roxbyite phases exhibited greater catalytic ability than the djulerite phases, with 90% and 99% degradation for Cu_7S_4 (220 °C) and Cu_7S_4 (250 °C) respectively, which could be ascribed to the higher crystallinity of the roxbyite phase at 250 °C. The djulerite phases at 120 and 150 °C showed lower degradation percentages of 70% and 85%, respectively. Therefore, there seemed to be a direct relationship between the temperature and degradation efficiencies, and the degradation performance of these photocatalysts toward tetracycline molecules could be placed in the order $\text{Cu}_{31}\text{S}_{16}$ (120 °C) < $\text{Cu}_{31}\text{S}_{16}$

(150 °C) < Cu₇S₄ (220 °C) < Cu₇S₄ (250 °C). In addition to the crystallinity, the higher absorption properties observed in the spectra of the roxbyite phases could be responsible for the higher photocatalytic activities [51] and faster mineralization rate compared to the djulerite phases [50]. Due to the high degradation efficiency of the Cu₇S₄ (250 °C), subsequent degradation experiments for further studies were limited to this phase.

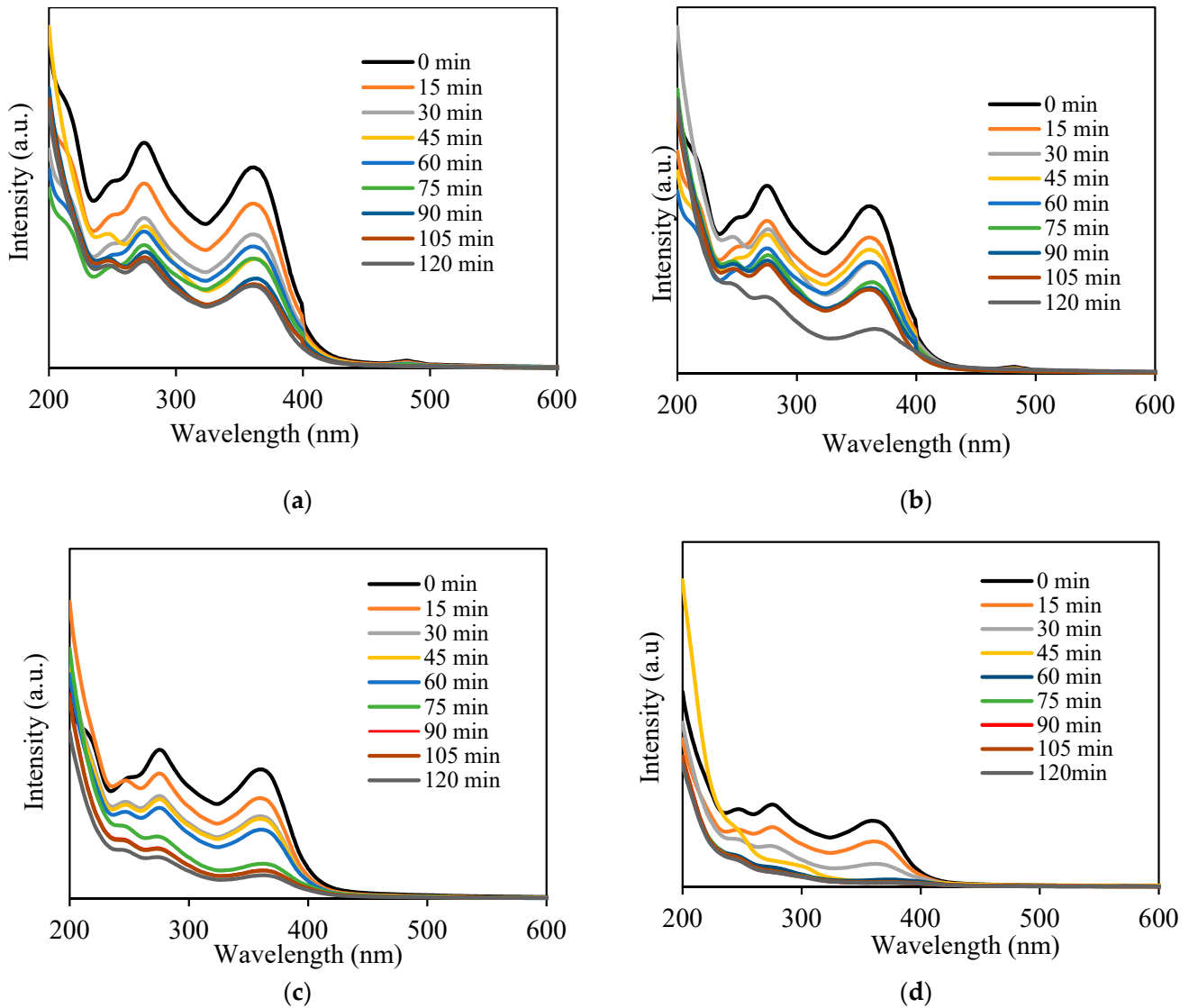


Figure 5. Photocatalytic degradation of tetracycline under visible light irradiation using (a) Cu₃₁S₁₆ (120 °C), (b) Cu₃₁S₁₆ (150 °C), (c) Cu₇S₄ (220 °C), and (d) Cu₇S₄ (250 °C).

2.4.2. Effect of TC Solution pH on the Degradation Efficiency

The initial pH of solution is one of the important parameters that influences the photocatalytic processes of compounds through the surface electrical charge characteristics of photocatalysts, and it dictates the ionization state of the catalyst surface. The effect of the solution's pH was studied using 50 mg/L concentrations of TC, 80 mg of Cu₇S₄ (250 °C), and solution pH in the range of 2–10. Figure 6 presents the removal efficiencies at different irradiation times up to 120 min. The degradation efficiency obtained at pH 4 was 99%, while those obtained at pH 2, 6, 8, and 10 were 73.4%, 62.3%, 54.1%, and 46.7%, respectively. In addition, the outcome showed a decrease in percentage degradation of TC from 99% to 46.7% with the increase in the pH of the solution, indicating that pH 4 was the optimum [52]. Alkaline pH values (8 and 10) adversely affected the photocatalytic

degradation of TC, resulting in a decrease in the removal efficiency up to 46.7%. The decrease in removal efficiency of TC in the alkaline pH range could be attributed to the concentration of hydroxyl radical, which was influenced by the solution pH. Perhaps the pH of the TC solution had a significant effect on the surface ionic speciation of the Cu_7S_4 and was able to control the reactants type and products obtained in the process. Similar results were reported by Ahmadi et al. [53], and Hao et al. [54] reported their studies on the photocatalytic degradation of TC using different photocatalysts. However, the influence of solution pH 2 on the degradation process was not very clear, because no direct trend could be established on the basis of the acidity and alkalinity of the solution [55].

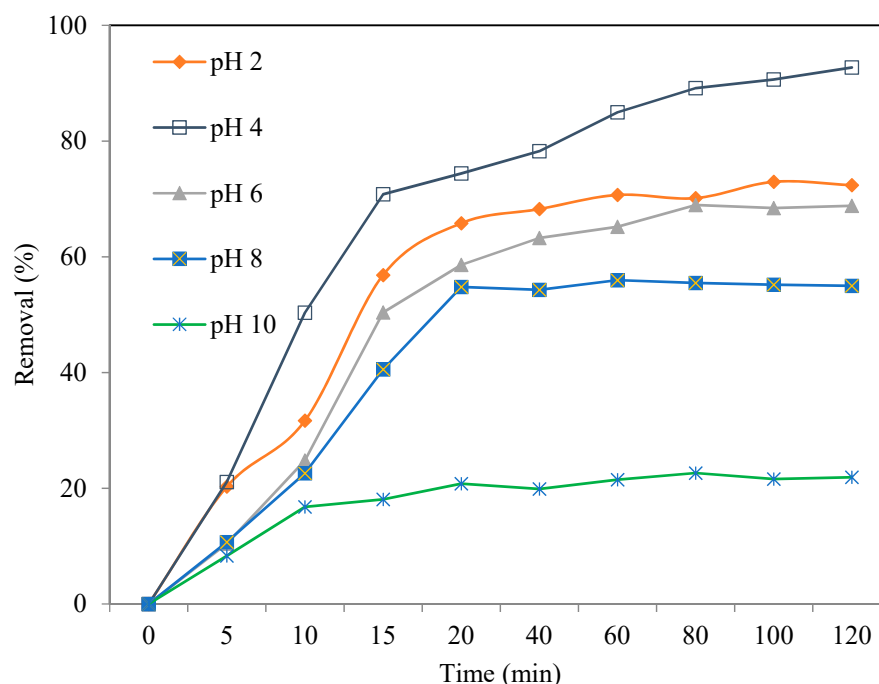


Figure 6. Effect of TC solution pH on Cu_7S_4 (250 °C) (dosage: 80 mg/L, irradiation time: 120 min, TC: 50 mg/L).

2.4.3. Effect of Catalysts (Cu_7S_4 (250 °C) Loading)

The degradation of TC was conducted under the visible light irradiation in the absence of the photocatalyst, and very little (3%) degradation of TC could be observed after 120 min reaction, as presented in Figure 7. The removal of TC using different catalyst loading at pH 4 and TC concentration of 50 mg/L under the visible light was conducted afterwards. An increase in the degradation rate constants with an increase in catalyst loading from 5 to 80 mg occurred, with about 99.1% and 25% degradation efficiencies achieved with 80 mg and 5 mg of Cu_7S_4 (250 °C), respectively. The increase in degradation of TC with increasing concentration of Cu_7S_4 (250 °C) in the solution could be ascribed to the increasing availability of more active sites, higher formation of OH, and increased effective interaction of the catalyst with the TC molecules. However, at a higher catalyst loading above 80 mg, most of the catalyst may suffer deactivation due to their accumulation, agglomeration, or precipitation, which could lead to a decrease in the available catalyst surface for light absorption and consequently result in a decrease in the degradation rate. Although catalyst loading above 80 mg was not investigated, Figure 7 shows almost 100% degradation of TC using 80 mg, indicating an optimal or equilibrium dosage for TC in this operating condition. These results were in accordance with some earlier reported studies involving the degradation performances of copper sulfide [56,57].

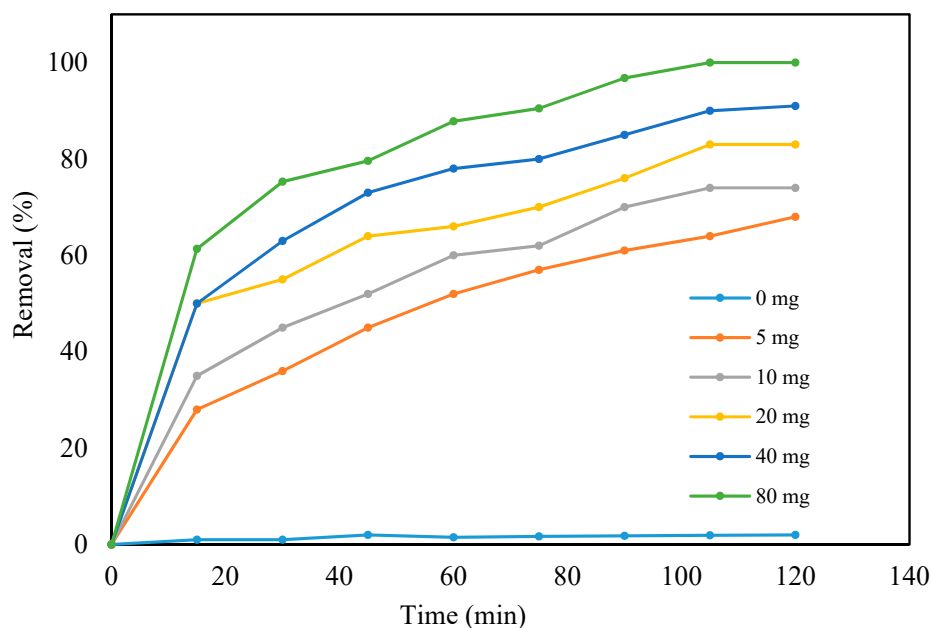


Figure 7. The effect of catalyst loading on the photoreduction of TC using Cu_7S_4 ($250\text{ }^\circ\text{C}$) as a photocatalyst.

2.4.4. Effect of Initial Concentration of TC

The effect of initial TC concentration on the removal efficiency of Cu_7S_4 ($250\text{ }^\circ\text{C}$) was investigated and presented in Figure 8. The rate of degradation could be determined by the formation of hydroxyl radicals at any TC concentration. It could be observed that the removal efficiency of the photocatalyst decreased with increase in the initial TC concentrations from 5 to 25 mg/L after 120 min, which reflected the lower removal efficiency at higher TC concentrations. Thus, this implies that the rate of the TC degradation will decrease with the increase in the initial TC concentration, which could be due to the fact that the concentration of generated $\bullet\text{OH}$ on the surface of the photocatalyst will decrease as more TC ions cover the active sites of the photocatalyst. Furthermore, there will be an increase in the concentration of TC molecules adsorbed on the surface of the photocatalyst as the initial TC concentration increased. The high concentration of adsorbed TC resulted in an inhibitive effect on the reaction of TC molecules with photogenerated holes or hydroxyl radicals due to the lack of any direct contact between them [58]. The increase in internal optical density makes the solution become impervious to visible light, which is another reason for obtaining lower degradation efficiency at higher TC concentration. In addition, increasing the TC concentration, which led to the absorption of light by the TC molecules, could also hinder the photons from reaching the photocatalyst surface, thereby decreasing the photocatalytic removal efficiency [59]. The equal amount of reactive radicals formed in all concentrations might lead to an increased reaction of TC molecules with radicals at lower TC concentrations. This could also result in a decrease in the degradation [60]. The reusability of Cu_7S_4 ($250\text{ }^\circ\text{C}$) was evaluated in order to determine its long-term use as a photocatalyst in the removal of TC. These experiments were conducted by repeating the degradation studies of TC using a solution of 25 mg/L. Figure 9 displays the recyclability of Cu_7S_4 ($250\text{ }^\circ\text{C}$) for four cycles, and the results showed that the photocatalyst could be reused effectively after four cycles with little loss in activity. Thus, industrial application of this product is highly viable due to its reusability and stability properties. Similar results were reported in the studies related to the photo degradation of antibiotics [61,62].

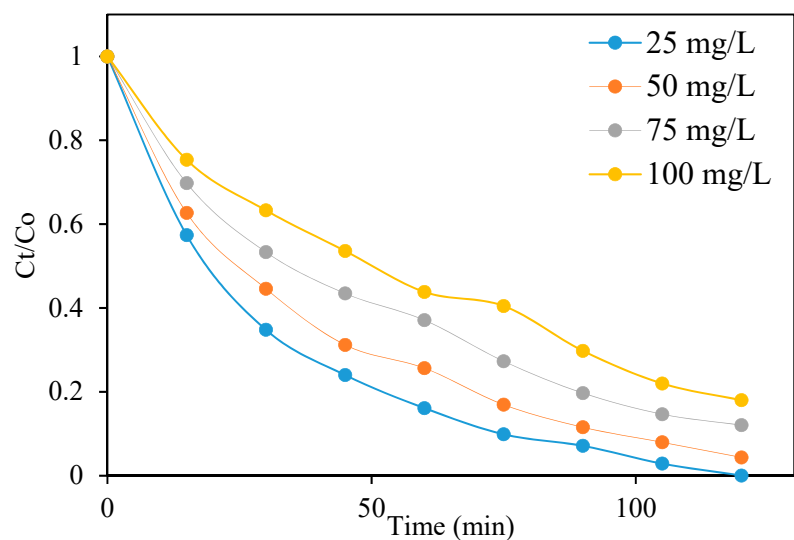


Figure 8. Effect of TC concentration on Cu_7S_4 (250 °C) (dosage: 80 mg, irradiation time: 120 min, pH: 4).

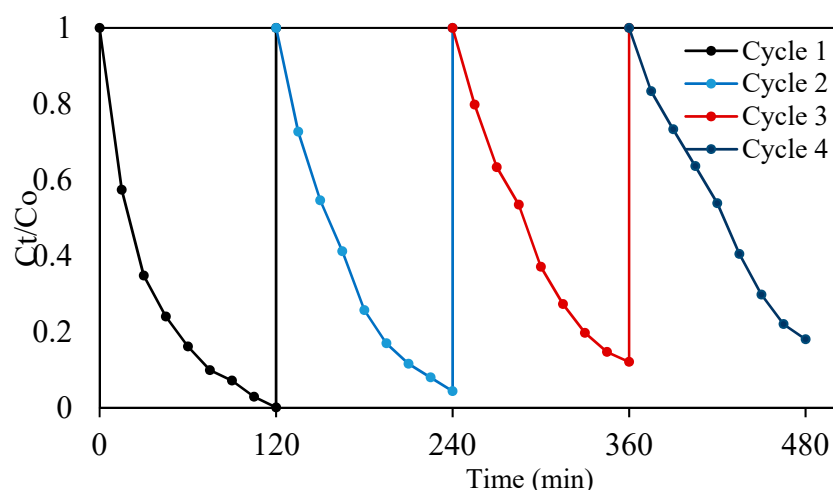


Figure 9. Reusability cycles of TC degradation using Cu_7S_4 (250 °C) nanocomposite and a solution of 25 mg/L TC.

Photocatalytic Degradation Mechanism

Based on the obtained results and other related studies [16,63], the possible mechanism involved in the photocatalytic degradation of TC under visible light has been proposed and presented in Figure 10. Upon the irradiation of Cu_7S_4 , the photocatalysts are excited, leading to the generation of photogenerated electron-hole pairs that have strong reducing and oxidizing powers, respectively. The photo-induced electron-hole pairs are transferred to the surface of the photocatalysts and could directly be involved in the photocatalytic reaction process or produce active radicals [64]. In general, hydroxyl radicals ($\cdot\text{OH}$), superoxide radicals ($\cdot\text{O}_2^-$), and holes (h^+) can be found in the photocatalytic degradation process. Since the redox potential of the LUMO of Cu_7S_4 was more negative than that of $\text{O}_2/\cdot\text{O}_2^-$ ($E_0 = -0.33 \text{ eV/NHE}$), the dissolved O_2 can interact with the photoelectrons on the LUMO. This leads to the generation of $\cdot\text{O}_2^-$ radicals and the charge carrier separation. The photogenerated holes can react with H_2O to form hydroxyl radicals ($\cdot\text{OH}$). Finally, ($\cdot\text{O}_2^-$) and ($\cdot\text{OH}$) degrade TC into other products, as shown in Figure 10.

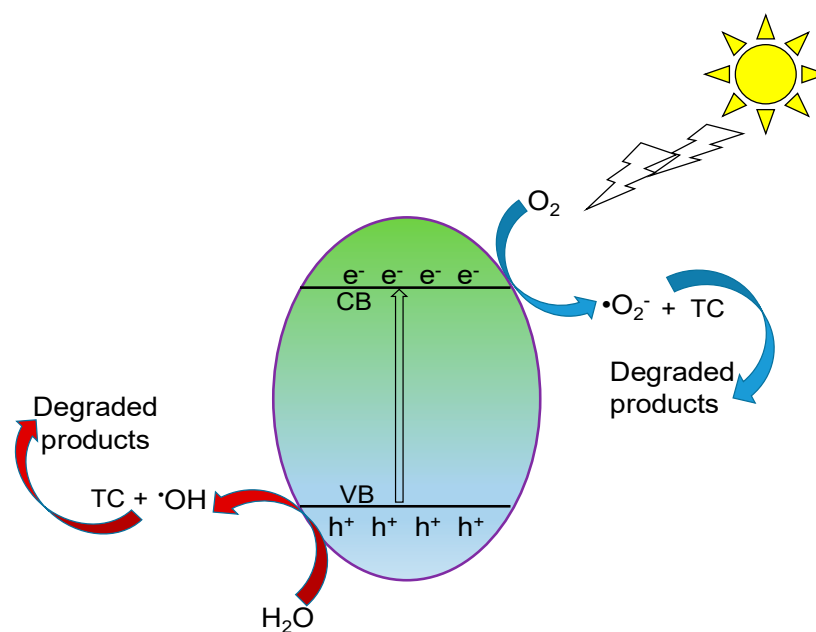


Figure 10. The schematic representation of the possible photocatalytic mechanism involved in the degradation of TC under visible light irradiation.

3. Materials and Methods

3.1. Preparation of Copper Dithiocarbamate Complex

The copper complex was prepared using an already reported procedure [36]. Briefly, a methanol solution featured an equimolar ratio of 4-ethylamine and p-tolualdehyde (4.0 mmol) mixed together and stirred at room temperature for 2 h. Thereafter, the solvent was removed, and the resulting oily product was dissolved in an equivolume solution of methanol and dichloromethane. Sodium borohydride was added and stirred for another 2 h in ice, and the solution was stirred for 20 h at room temperature, which was followed by the removal of the solvent. The product was rinsed with water and extracted with dichloromethane. Then, the organic layer was evaporated to afford the substituted amine as a brownish oil, which was dissolved in ethanol and followed by the addition of potassium hydroxide. The solution was stirred for 30 min, and carbon disulfide was added dropwise while maintaining the temperature for 2 h. To this solution, a stoichiometric amount of copper(II) chloride dihydrate was added, and the resulting copper dithiocarbamate precipitates were rinsed using cold water and then air-dried.

3.2. Preparation of Copper Sulfide Nanoparticles

Copper sulfide nanoparticles were prepared via a solvothermal reaction under N_2 atmosphere using a heat-up method. In a round-bottom flask with a condenser, 0.75 g of copper(II) bis(*N*-4-methylbenzyl)-*N*-(4-ethylphenyl) dithiocarbamate was added into 20 mL of dodecanthiol. After degassing, the mixture was heated at a steady temperature up to 120 °C and maintained for 1 h. Afterwards, the dark solution was left to cool down to room temperature. Then, the obtained product was separated by the addition of ethanol and centrifugation. To purify the product, ethanol and toluene (1:3 v/v) were used to wash the product 3 times. The procedure was repeated while the temperature of the reaction was changed to 150, 180, 220, and 250 °C respectively.

3.3. Characterization of the Prepared Samples

The X-ray powder diffraction data were collected on a Bruker D8 Advanced, which utilizes $CuK\alpha$ radiation (wavelength, $\lambda = 1.5406 \text{ \AA}$) with variable slits at 45 kV/40 Ma. Scanning electron microscope (SEM) measurement was carried out on a JOEL JSM-6390 LVSEM fitted with an energy-dispersive X-ray spectrometer (EDAX) for the elemental

analysis of the samples. The internal morphology of the nanoparticles was studied using a TECNAI G2 (ACI) TEM equipped with a CCD camera and operating at a voltage of 120 kV. The optical properties of the nanoparticles were studied using a Jobin Yvon LabRAM HR 800 UV/Vis/NIR spectrophotometer and a Perkin Elmer L45 photoluminescence spectrometer for the absorption and fluorescence measurement.

3.4. Photocatalytic Evaluation

In the photocatalytic experiment, an LED visible light lamp ($\lambda > 420$ nm) was used as the light source. Firstly, about 80 mg of each catalyst was added to 100 mL of TC solution containing 50 mg/L TC in a 200 mL flask, and the solution was magnetically stirred in the dark for 60 min in order to achieve adsorption–desorption equilibrium. Then, the light source was turned on in order to initiate the photocatalytic reaction. As the reaction progressed, approximately 5 mL of suspension was collected every 15 min and filtered through 0.22 μ m PTFE syringe filters. The obtained clear solution was introduced into a quartz cuvette, and the absorbance of the TC was measured using an ultraviolet–visible spectrophotometer. The concentration of the TC degraded was calculated using the formula given in Equation (1).

$$DR(\%) = \frac{C_0 - C_i}{C_0} \times 100\% = \frac{A_0 - A_i}{A_0} \times 100(\%) \quad (1)$$

where C_i is the concentration of TC at different times; C_0 is the initial concentration of TC; A_i is the TC absorbance at different times; and A_0 is the blank absorbance of the original TC solution.

4. Conclusions

In summary, a simple one-pot solvothermal route was used to prepare pure phase copper sulfide nanoparticles by variation in the reaction temperature, resulting in phase transformation from djurleite ($\text{Cu}_{31}\text{S}_{16}$) to roxbyite phase as the temperature increased from 120 to 250 °C. No morphological changes accompanied the phase transformation process even after increasing the reaction temperature to 250 °C. An observable increase in particle size occurred, which was induced by temperature increase, and the optical characterization showed a band-gap energy in the range of 1.34–2.20 eV. The photocatalytic degradation of TC using the synthesized pure djurleite and roxbyite phases showed photocatalytic activities, with Cu_7S_4 (250 °C) exhibiting the greatest efficiency of 99% at pH 4 compared to the performances achieved using the other samples (Cu_7S_4 (220 °C), djurleite $\text{Cu}_{31}\text{S}_{16}$ (150 °C), and $\text{Cu}_{31}\text{S}_{16}$ (120 °C)). The photocatalytic experimental data conform to a pseudo-second-order kinetics model with a higher correlation factor. This is an indication that the interaction between TC and copper sulfide nanoparticles is based on a chemical reaction. Overall, roxbyite (Cu_7S_4) could be considered as a potential catalyst for the degradation of TC in solution.

Author Contributions: Writing—original draft, investigation, methodology, M.P.R.; Conceptualization, writing—review and editing, D.C.O.; formal analysis, writing—review and editing, O.A.O.; formal analysis, writing—review and editing, S.R.; formal analysis, writing—review and editing, L.M. All authors have read and agreed to the published version of the manuscript.

Funding: The authors acknowledge the financial support from North-West University, South and the payment of the APC.

Acknowledgments: The authors gratefully acknowledge the North-West University and the National Research Foundation, South Africa for providing financial assistance.

Conflicts of Interest: The authors declare no conflict of interest.

References

1. Cully, M. Public health: The politics of antibiotics. *Nature* **2014**, *509*, S16–S17. [[CrossRef](#)]
2. Cheng, D.; Ngo, H.H.; Guo, W.; Chang, S.W.; Nguyen, D.D.; Liu, Y.; Wei, Q.; Wei, D. A critical review on antibiotics and hormones in swine wastewater: Water pollution problems and control approaches. *J. Hazard. Mater.* **2020**, *387*, 121682. [[CrossRef](#)]
3. Pan, Y.; Zhang, Y.; Zhou, M.; Cai, J.; Tian, Y. Enhanced removal of antibiotics from secondary wastewater effluents by novel UV/pre-magnetized Fe⁰/H₂O₂ process. *Water Res.* **2019**, *153*, 144–159. [[CrossRef](#)]
4. Wang, J.; Zhuan, R. Degradation of antibiotics by advanced oxidation processes: An overview. *Science of The Total Environment* **2020**, *701*, 135023. [[CrossRef](#)]
5. Kumar, M.; Jaiswal, S.; Sodhi, K.K.; Shree, P.; Singh, D.K.; Agrawal, P.K.; Shukla, P. Antibiotics bioremediation: Perspectives on its ecotoxicity and resistance. *Environ. Int.* **2019**, *124*, 448–461. [[CrossRef](#)]
6. De Cazes, M.; Belleville, M.-P.; Petit, E.; Llorca, M.; Rodríguez-Mozaz, S.; De Gunzburg, J.; Barceló, D.; Sanchez-Marcano, J. Design and optimization of an enzymatic membrane reactor for tetracycline degradation. *Catal. Today* **2014**, *236*, 146–152. [[CrossRef](#)]
7. Tong, X.; Mao, M.; Xie, J.; Zhang, K.; Xu, D. Insights into the interactions between tetracycline, its degradation products and bovine serum albumin. *SpringerPlus* **2016**, *5*, 1–9. [[CrossRef](#)] [[PubMed](#)]
8. Ji, Y.; Shi, Y.; Dong, W.; Wen, X.; Jiang, M.; Lu, J. Thermo-activated persulfate oxidation system for tetracycline antibiotics degradation in aqueous solution. *Chem. Eng. J.* **2016**, *298*, 225–233. [[CrossRef](#)]
9. Gu, C.; Karthikeyan, K. Interaction of tetracycline with aluminum and iron hydrous oxides. *Environ. Sci. Technol.* **2005**, *39*, 2660–2667. [[CrossRef](#)] [[PubMed](#)]
10. Xiong, H.; Zou, D.; Zhou, D.; Dong, S.; Wang, J.; Rittmann, B.E. Enhancing degradation and mineralization of tetracycline using intimately coupled photocatalysis and biodegradation (ICPB). *Chem. Eng. J.* **2017**, *316*, 7–14. [[CrossRef](#)]
11. Zhu, X.; Liu, Y.; Zhou, C.; Luo, G.; Zhang, S.; Chen, J. A novel porous carbon derived from hydrothermal carbon for efficient adsorption of tetracycline. *Carbon* **2014**, *77*, 627–636. [[CrossRef](#)]
12. Zhu, X.-D.; Wang, Y.-J.; Sun, R.-J.; Zhou, D.-M. Photocatalytic degradation of tetracycline in aqueous solution by nanosized TiO₂. *Chemosphere* **2013**, *92*, 925–932. [[CrossRef](#)]
13. Liu, M.; An, D.; Hou, L.; Yu, S.; Zhu, Y. Zero valent iron particles impregnated zeolite X composites for adsorption of tetracycline in aquatic environment. *RSC Adv.* **2015**, *5*, 103480–103487. [[CrossRef](#)]
14. Chen, X.; Jiang, X.; Yin, C.; Zhang, B.; Zhang, Q. Facile fabrication of hierarchical porous ZIF-8 for enhanced adsorption of antibiotics. *J. Hazard. Mater.* **2019**, *367*, 194–204. [[CrossRef](#)] [[PubMed](#)]
15. Zhao, Y.; Ye, M.; Zhang, X.; Sun, M.; Zhang, Z.; Chao, H.; Huang, D.; Wan, J.; Zhang, S.; Jiang, X. Comparing polyvalent bacteriophage and bacteriophage cocktails for controlling antibiotic-resistant bacteria in soil-plant system. *Sci. Total. Environ.* **2019**, *657*, 918–925. [[CrossRef](#)]
16. Safari, G.H.; Hoseini, M.; Seyedsalehi, M.; Kamani, H.; Jaafari, J.; Mahvi, A.H. Photocatalytic degradation of tetracycline using nanosized titanium dioxide in aqueous solution. *Int. J. Environ. Sci. Technol.* **2015**, *12*, 603–616. [[CrossRef](#)]
17. Wang, X.; Liu, Q.; Yang, Q.; Zhang, Z.; Fang, X.J.C. Three-dimensional g-C₃N₄ aggregates of hollow bubbles with high photocatalytic degradation of tetracycline. *Carbon* **2018**, *136*, 103–112. [[CrossRef](#)]
18. Ahadi, M.; Tehrani, M.S.; Azar, P.A.; Husain, S.W. Novel preparation of sensitized ZnS nanoparticles and its use in photocatalytic degradation of tetracycline. *Int. J. Environ. Sci. Technol.* **2016**, *13*, 2797–2804. [[CrossRef](#)]
19. Yan, M.; Yan, Y.; Wu, Y.; Shi, W.; Hua, Y.J.R.a. Microwave-assisted synthesis of monoclinic–tetragonal BiVO₄ heterojunctions with enhanced visible-light-driven photocatalytic degradation of tetracycline. *SC Adv.* **2015**, *5*, 90255–90264. [[CrossRef](#)]
20. Jingyu, H.; Ran, Y.; Zhaohui, L.; Yuanqiang, S.; Lingbo, Q.; Kani, A.N. In-situ growth of ZnO globular on g-C₃N₄ to fabrication binary heterojunctions and their photocatalytic degradation activity on tetracyclines. *Solid State Sci.* **2019**, *92*, 60–67. [[CrossRef](#)]
21. Khodadadi, M.; Panahi, A.H.; Al-Musawi, T.J.; Ehrampoush, M.H.; Mahvi, A.H. The catalytic activity of FeNi₃@SiO₂ magnetic nanoparticles for the degradation of tetracycline in the heterogeneous Fenton-like treatment method. *J. Water Proc. Eng.* **2019**, *32*, 100943. [[CrossRef](#)]
22. Niu, J.; Ding, S.; Zhang, L.; Zhao, J.; Feng, C.J.C. Visible-light-mediated Sr-Bi₂O₃ photocatalysis of tetracycline: Kinetics, mechanisms and toxicity assessment. *Chemosphere* **2013**, *93*, 1–8. [[CrossRef](#)] [[PubMed](#)]
23. Zhang, K.; Gu, S.; Wu, Y.; Fan, Q.; Zhu, C. Preparation of pyramidal SnO/CeO₂ nano-heterojunctions with enhanced photocatalytic activity for degradation of tetracycline. *Nanotechnology* **2020**, *31*, 215702. [[CrossRef](#)] [[PubMed](#)]
24. Semeraro, P.; Bettini, S.; Sawalha, S.; Pal, S.; Licciulli, A.; Marzo, F.; Lovergine, N.; Valli, L.; Giancane, G.J.N. Photocatalytic degradation of tetracycline by ZnO/γ-Fe₂O₃ paramagnetic nanocomposite material. *Nanomaterials* **2020**, *10*, 1458. [[CrossRef](#)] [[PubMed](#)]
25. Cao, M.; Wang, P.; Ao, Y.; Wang, C.; Hou, J.; Qian, J. Visible light activated photocatalytic degradation of tetracycline by a magnetically separable composite photocatalyst: Graphene oxide/magnetite/cerium-doped titania. *J. Colloid Interface Sci.* **2016**, *467*, 129–139. [[CrossRef](#)]
26. Lai, C.; Xu, F.; Zhang, M.; Li, B.; Liu, S.; Yi, H.; Li, L.; Qin, L.; Liu, X.; Fu, Y.J.J.O.C.; et al. Facile synthesis of CeO₂/carbonate doped Bi₂O₂CO₃ Z-scheme heterojunction for improved visible-light photocatalytic performance: Photodegradation of tetracycline and photocatalytic mechanism. *J. Colloid Interface Sci.* **2021**, *588*, 283–294. [[CrossRef](#)]

27. Liu, Y.; Kong, J.; Yuan, J.; Zhao, W.; Zhu, X.; Sun, C.; Xie, J.J.C.E.J. Enhanced photocatalytic activity over flower-like sphere Ag/Ag₂CO₃/BiVO₄ plasmonic heterojunction photocatalyst for tetracycline degradation. *Chem. Eng. J.* **2018**, *331*, 242–254. [[CrossRef](#)]
28. Lv, C.; Lan, X.; Wang, L.; Dai, X.; Zhang, M.; Cui, J.; Yuan, S.; Wang, S.; Shi, J.J.E.t. Rapidly and highly efficient degradation of tetracycline hydrochloride in wastewater by 3D IO-TiO₂-CdS nanocomposite under visible light. *Environ. Technol.* **2021**, *42*, 377–387. [[CrossRef](#)] [[PubMed](#)]
29. Page, M.; Niitsoo, O.; Itzhaik, Y.; Cahen, D.; Hodes, G.J.E.; Science, E. Copper sulfide as a light absorber in wet-chemical synthesized extremely thin absorber (ETA) solar cells. *Energy Environ. Sci.* **2009**, *2*, 220–223. [[CrossRef](#)]
30. Isac, L.; Duta, A.; Kriza, A.; Manolache, S.; Nanu, M. Copper sulfides obtained by spray pyrolysis—possible absorbers in solid-state solar cells. *Thin Solid Film.* **2007**, *515*, 5755–5758. [[CrossRef](#)]
31. Khan, M.D.; Akhtar, J.; Malik, M.A.; Revaprasadu, N. Tuning the phase and shape of copper sulfide nanostructures using mixed solvent systems. *Chem. Sel.* **2016**, *1*, 5982–5989. [[CrossRef](#)]
32. Ueda, H.; Nohara, M.; Kitazawa, K.; Takagi, H.; Fujimori, A.; Mizokawa, T.; Yagi, T. Copper pyrites CuS₂ and CuSe₂ as anion conductors. *Phys. Rev. B* **2002**, *65*, 155104. [[CrossRef](#)]
33. Mulder, B.J. Optical properties of crystals of cuprous sulphides (chalcosite, djurleite, Cu_{1.9}S, and digenite). *Phys. Status Solidi* **1972**, *13*, 79–88. [[CrossRef](#)]
34. Schneider, N.; Lincot, D.; Donsanti, F. Atomic layer deposition of copper sulfide thin films. *Thin Solid Film.* **2016**, *600*, 103–108. [[CrossRef](#)]
35. Ravele, M.P.; Oyewo, O.A.; Onwudiwe, D.C. Controlled Synthesis of CuS and Cu₉S₅ and Their Application in the Photocatalytic Mineralization of Tetracycline. *Catalysts* **2021**, *11*, 899. [[CrossRef](#)]
36. Akhtar, M.; Alghamdi, Y.; Akhtar, J.; Aslam, Z.; Revaprasadu, N.; Malik, M.A. Phase controlled synthesis of copper sulfide nanoparticles by colloidal and non-colloidal methods. *Mater. Chem. Phys.* **2016**, *180*, 404–412. [[CrossRef](#)]
37. Qin, Y.; Li, X.; Liu, W.; Lei, X. High-performance aqueous polysulfide-iodide flow battery realized by an efficient bifunctional catalyst based on copper sulfide. *Mater. Today Energy* **2021**, *21*, 100746. [[CrossRef](#)]
38. Jiao, S.; Xu, L.; Jiang, K.; Xu, D. Well-defined non-spherical copper sulfide mesocages with single-crystalline shells by shape-controlled Cu₂O crystal templating. *Adv. Mater.* **2006**, *18*, 1174–1177. [[CrossRef](#)]
39. Shen, S.; Zhang, Y.; Peng, L.; Xu, B.; Du, Y.; Deng, M.; Xu, H.; Wang, Q. Generalized synthesis of metal sulfide nanocrystals from single-source precursors: Size, shape and chemical composition control and their properties. *CrystEngComm* **2011**, *13*, 4572–4579. [[CrossRef](#)]
40. Zhuang, Z.; Peng, Q.; Li, Y. Controlled synthesis of semiconductor nanostructures in the liquid phase. *Chem. Soc. Rev.* **2011**, *40*, 5492–5513. [[CrossRef](#)] [[PubMed](#)]
41. Wang, Y.; Tang, A.; Li, K.; Yang, C.; Wang, M.; Ye, H.; Hou, Y.; Teng, F. Shape-controlled synthesis of PbS nanocrystals via a simple one-step process. *Langmuir* **2012**, *28*, 16436–16443. [[CrossRef](#)] [[PubMed](#)]
42. Olalekan, O.C.; Onwudiwe, D.C. Temperature controlled evolution of pure phase Cu₉S₅ nanoparticles by solvothermal process. *Front. Mater.* **2021**. [[CrossRef](#)]
43. Zhang, S.; Meng, W.; Wang, L.; Li, L.; Long, Y.; Hei, Y.; Zhou, L.; Wu, S.; Zheng, Z.; Luo, L.; et al. Preparation of Nano-Copper Sulfide and Its Adsorption Properties for 17 α -Ethinyl Estradiol. *Nanoscale Res. Lett.* **2020**, *15*, 48. [[CrossRef](#)] [[PubMed](#)]
44. Zhao, Y.; Pan, H.; Lou, Y.; Qiu, X.; Zhu, J.; Burda, C. Plasmonic Cu₂-xS nanocrystals: Optical and structural properties of copper-deficient copper (I) sulfides. *J. Am. Chem. Soc.* **2009**, *131*, 4253–4261. [[CrossRef](#)]
45. Partain, L.; McLeod, P.; Duisman, J.; Peterson, T.; Sawyer, D.; Dean, C. Degradation of a Cu x S/CdS solar cell in hot, moist air and recovery in hydrogen and air. *J. Appl. Phys.* **1983**, *54*, 6708–6720. [[CrossRef](#)]
46. Aftab, M.; Butt, M.; Ali, D.; Bashir, F.; Khan, T.M. Optical and electrical properties of NiO and Cu-doped NiO thin films synthesized by spray pyrolysis. *Opt. Mater.* **2021**, *119*, 111369. [[CrossRef](#)]
47. Mulder, B. Optical properties and energy band scheme of cuprous sulphides with ordered and disordered copper ions. *Phys. Status Solidi* **1973**, *18*, 633–638. [[CrossRef](#)]
48. Behboudnia, M.; Khanbabaee, B. Investigation of nanocrystalline copper sulfide Cu₇S₄ fabricated by ultrasonic radiation technique. *J. Cryst. Growth* **2007**, *304*, 158–162. [[CrossRef](#)]
49. Abdelhady, A.L.; Ramasamy, K.; Malik, M.A.; O'Brien, P.; Haigh, S.J.; Raftery, J. New routes to copper sulfide nanostructures and thin films. *J. Mater. Chem.* **2011**, *21*, 17888–17895. [[CrossRef](#)]
50. Wu, S.; Hu, H.; Lin, Y.; Zhang, J.; Hu, Y.H. Visible light photocatalytic degradation of tetracycline over TiO₂. *Chem. Eng. J.* **2020**, *382*, 122842. [[CrossRef](#)]
51. Wang, D.; Jia, F.; Wang, H.; Chen, F.; Fang, Y.; Dong, W.; Zeng, G.; Li, X.; Yang, Q.; Yuan, X. Simultaneously efficient adsorption and photocatalytic degradation of tetracycline by Fe-based MOFs. *J. Colloid Interface Sci.* **2018**, *519*, 273–284. [[CrossRef](#)] [[PubMed](#)]
52. Nasseh, N.; Barikbin, B.; Taghavi, L. Photocatalytic degradation of tetracycline hydrochloride by FeNi₃/SiO₂/CuS magnetic nanocomposite under simulated solar irradiation: Efficiency, stability, kinetic and pathway study. *Environ. Technol. Innov.* **2020**, *20*, 101035. [[CrossRef](#)]
53. Ahmadi, M.; Motlagh, H.R.; Jaafarzadeh, N.; Mostoufi, A.; Saeedi, R.; Barzegar, G.; Jorfi, S.J.J. Enhanced photocatalytic degradation of tetracycline and real pharmaceutical wastewater using MWCNT/TiO₂ nano-composite. *J. Environ. Manag.* **2017**, *186*, 55–63. [[CrossRef](#)]

54. Hao, R.; Xiao, X.; Zuo, X.; Nan, J.; Zhang, W.J.J.o.h.m. Efficient adsorption and visible-light photocatalytic degradation of tetracycline hydrochloride using mesoporous BiOI microspheres. *J. Hazard. Mater.* **2012**, *209*, 137–145. [[CrossRef](#)] [[PubMed](#)]
55. Nasseh, N.; Taghavi, L.; Barikbin, B.; Nasser, M.A. Synthesis and characterizations of a novel FeNi₃/SiO₂/CuS magnetic nanocomposite for photocatalytic degradation of tetracycline in simulated wastewater. *J. Clean. Prod.* **2018**, *179*, 42–54. [[CrossRef](#)]
56. Kundu, J.; Pradhan, D. Controlled Synthesis and Catalytic Activity of Copper Sulfide Nanostructured Assemblies with Different Morphologies. *ACS Appl. Mater. Interfaces* **2014**, *6*, 1823–1834. [[CrossRef](#)]
57. Chen, Y.; Chen, K.; Fu, J.; Yamaguchi, A.; Li, H.; Pan, H.; Hu, J.; Miyauchi, M.; Liu, M. Recent advances in the utilization of copper sulfide compounds for electrochemical CO₂ reduction. *Nano Mater. Sci.* **2020**, *2*, 235–247. [[CrossRef](#)]
58. Ahmad, F.; Zhu, D.; Sun, J. Environmental fate of tetracycline antibiotics: Degradation pathway mechanisms, challenges, and perspectives. *Environ. Sci. Eur.* **2021**, *33*, 64. [[CrossRef](#)]
59. Dai, J.; Sun, Y.; Liu, Z. Efficient degradation of tetracycline in aqueous solution by Ag/AgBr catalyst under solar irradiation. *Mater. Res. Express* **2019**, *6*, 085512. [[CrossRef](#)]
60. Farzaneh, S.; Keramati, N.; Ghazi, M.M. Optimization of Photocatalytic Degradation of Tetracycline Using Titania Based on Natural Zeolite by Response Surface Approach. *J. Water Chem. Technol.* **2020**, *42*, 30–35. [[CrossRef](#)]
61. Farzadkia, M.; Rahmani, K.; Gholami, M.; Esrafil, A.; Rahmani, A.; Rahmani, H.J.K.J.o.C.E. Investigation of photocatalytic degradation of clindamycin antibiotic by using nano-ZnO catalysts. *Korean J. Chem. Eng.* **2014**, *31*, 2014–2019. [[CrossRef](#)]
62. Zuo, S.; Chen, Y.; Liu, W.; Yao, C.; Li, X.; Li, Z.; Ni, C.; Liu, X.J.C.I. A facile and novel construction of attapulgite/Cu₂O/Cu/g-C₃N₄ with enhanced photocatalytic activity for antibiotic degradation. *Ceram. Int.* **2017**, *43*, 3324–3329. [[CrossRef](#)]
63. Hou, C.; Liu, H.; Li, Y.J.R.A. The preparation of three-dimensional flower-like TiO₂/TiOF₂ photocatalyst and its efficient degradation of tetracycline hydrochloride. *RSC Adv.* **2021**, *11*, 14957–14969. [[CrossRef](#)]
64. Jin, Y.; Jiang, D.; Li, D.; Chen, M. Construction of ultrafine TiO₂ nanoparticle and SnNb₂O₆ nanosheet 0D/2D heterojunctions with abundant interfaces and significantly improved photocatalytic activity. *Catal. Sci. Technol.* **2017**, *7*, 2308–2317. [[CrossRef](#)]